STRUCTURAL BIOLOGY
COMMUNICATIONS

ISSN: 2053-230X
journals.iucr.org/f

Crystal structure of an IclR homologue from *Microbacterium* sp. strain HM58-2

Tomonori Akiyama, Yusuke Yamada, Naoki Takaya, Shinsaku Ito, Yasuyuki Sasaki and Shunsuke Yajima

Acta Cryst. (2017). F**73**, 16–23

STRUCTURAL BIOLOGY COMMUNICATIONS

ISSN 2053-230X

Crystal structure of an IclR homologue from *Microbacterium* sp. strain HM58-2

Tomonori Akiyama,[a] Yusuke Yamada,[b] Naoki Takaya,[c] Shinsaku Ito,[a] Yasuyuki Sasaki[a] and Shunsuke Yajima[a]*

[a]Department of Bioscience, Tokyo University of Agriculture, Setagaya-ku, Tokyo 156-8502, Japan, [b]Structural Biology Research Center, Photon Factory, Institute of Materials Structure Science, High Energy Accelerator Research Organization, 1-1 Oho, Tsukuba 305-0801, Japan, and [c]Department of Environmental and Life Sciences, Tsukuba University, Tennodai, Tsukuba, Japan. *Correspondence e-mail: yshun@nodai.ac.jp

Received 1 November 2016
Accepted 2 December 2016

Edited by A. Nakagawa, Osaka University, Japan

Keywords: isocitrate lyase regulator; transcription factor; *Microbacterium*; hydrazide; one-component system.

PDB reference: Mi-IclR, 5h1a

Supporting information: this article has supporting information at journals.iucr.org/f

The bacterial transcription factor IclR (isocitrate lyase regulator) is a member of a one-component signal transduction system, which shares the common motif of a helix–turn–helix (HTH)-type DNA-binding domain (DBD) connected to a substrate-binding domain (SBD). Here, the crystal structure of an IclR homologue (Mi-IclR) from *Microbacterium* sp. strain HM58-2, which catabolizes acylhydrazide as the sole carbon source, is reported. Mi-IclR is expected to regulate an operon responsible for acylhydrazide degradation as an initial step. Native single-wavelength anomalous diffraction (SAD) experiments were performed in combination with molecular replacement. *CRANK*2 from the *CCP*4 suite successfully phased and modelled the complete structure of a homotetramer composed of 1000 residues in an asymmetric unit, and the model was refined to 2.1 Å resolution. The overall structure of Mi-IclR shared the same domain combination as other known IclR structures, but the relative geometry between the DBD and SBD differs. Accordingly, the geometry of the Mi-IclR tetramer was unique: the putative substrate-binding site in each subunit is accessible from the outside of the tetramer, as opposed to buried inside as in the previously known IclR structures. These differences in the domain geometry may contribute to the transcriptional regulation of IclRs.

1. Introduction

Bacteria change their metabolic systems in response to environmental changes for their survival. In order to adapt their response, bacteria mainly use sensing mechanisms such as two-component systems (Stock *et al.*, 2000) and one-component systems (Ulrich *et al.*, 2005). IclR (isocitrate lyase regulator) is a member of a one-component system which regulates transcription. It was originally discovered and studied in *Escherichia coli* (Sunnarborg *et al.*, 1990). When *E. coli* grows in media with acetate or fatty acids as the sole carbon source, the glyoxylate bypass is induced. The *aceBAK* operon is expressed and regulated by the repressor IclR (Gui *et al.*, 1996). Currently, members of the IclR family have been identified in many bacteria. KdgR from *Erwinia chrysanthemi* and GylR from *Streptomyces coelicolor* as well as IclR from *E. coli* are known to be repressors, and an excess of specific substrate releases the repression of transcription (Molina-Henares *et al.*, 2006).

IclRs consist of 250–270 amino-acid residues, with a helix–turn–helix (HTH)-type DNA-binding domain (DBD) at the N-terminus connected by a short α-helix linker to a substrate-binding domain (SBD) at the C-terminus (Krell *et al.*, 2006).

Full-length crystal structures have been reported from *Thermotoga maritima* (TM0065; PDB entry 1mkm; Zhang *et al.*, 2002), *Rhodococcus* sp. RHA1 (PDB entries 2ia2, 2o0y and 2g7u; Midwest Center for Structural Genomics, unpublished work) and *Silicibacter* sp. TM1040 (PDB entry 3r4k; Joint Center for Structural Genomics, unpublished work). Their structures were homodimers or homotetramers. Two subunits cross at connected linker helices to form an X-shaped homodimer. The homotetramer is formed of a dimer of dimers. In relation to its role in one-component signal transduction systems, structures of complexes of IclR with specific substrates have also been reported, such as structures of the SBD from *E. coli* IclR complexed with pyruvate (PDB entry 2o9a) and glyoxylate (PDB entry 2o99) (Lorca *et al.*, 2007). However, no structures of complexes of full-length IclR have been reported to date.

Acylhydrazides, which are acylated derivatives of hydrazine, have the formula $R_1R_2N-N(R_3)C(=O)R_4$ and are organic compounds that are widely used to produce various materials in industrial applications, including for medicinal and agricultural uses. For example, they can act as antituberculosis agents (isonicotinic acid hydrazide; Scior *et al.*, 2002) or as antidepressants (isocarboxazid; López-Muñoz *et al.*, 2007). On the other hand, some natural compounds of this type are also known, such as agaritine from the commercial mushroom *Agaricus bisporus* (Levenberg, 1964) and gyromitrin from the poisonous false morel *Gyromitra esculenta* (Michelot & Toth, 1991). Despite the importance and the wide availability of acylhydrazide compounds, detailed analyses of the biological mechanism of the metabolic system of these compounds have not yet been performed. Recently, *Microbacterium* sp. strain HM58-2 was isolated using the acylhydrazide 4-hydroxybenzoic acid 1-phenylethylidene hydrazide (HBPH) as the sole carbon source, and hydrazidase was isolated as a key enzyme exhibiting hydrazide degradation (Oinuma *et al.*, 2015). Furthermore, expression of the hydrazidase gene was induced by HBPH when used as the sole carbon source. In the course of the elucidation of the hydrazide metabolic pathway in *Microbacterium* sp. HM58-2, the whole genome sequence of the bacterium was obtained, and it was revealed that the hydrazidase gene is located in an operon with an IclR-type transcription factor, which is expected to control the gene expression of the operon (Akiyama *et al.*, 2016).

In order to elucidate how IclR controls gene expression in this operon, we determined the crystal structure of IclR from *Microbacterium* sp. HM58-2 (Mi-IclR).

2. Materials and methods

2.1. Cloning, expression and purification of Mi-IclR

The IclR gene from *Microbacterium* sp. HM58-2 was amplified from its genomic DNA as a template using a primer set with forward primer 5′-CATATGGCCAATTCTCCGAGCGGC-3′ and reverse primer 5′-GAATTCCTACCAGCGCGAAGCGCGCA-3′; these sequences were obtained from the genome sequence (DDBJ/EMBL/GenBank accession No. BDCY01000009, locus tag MHM582_3486). Amplified fragments were cloned into pET-28b(+) using NdeI and EcoRI sites. Cloned vectors were transformed with the *E. coli* strain Arctic Express (DE3) and cultured in LB broth with 25 µg ml^{-1} kanamycin. After a 3 h culture at 37°C, the broth was cooled to 16°C and 100 µ*M* IPTG was added followed by a further 16 h culture. The purification of recombinant Mi-IclR was performed using an Ni–NTA column (Qiagen) equilibrated with buffer *A* (20 m*M* Tris–HCl pH 7.5, 100 m*M* NaCl, 10% glycerol) with 20 m*M* imidazole and eluted with buffer *A* with 500 m*M* imidazole. After dialysis against buffer *A*, the protein was concentrated to 10 mg ml^{-1} using Amicon Ultra-4 centrifugal filter units with molecular-weight cutoff 30 kDa (Merck Millipore).

Table 1
Data-collection and refinement statistics.

Data collection		
Beamline	PF-1A	PF-17A
Wavelength (Å)	2.700	1.038
Temperature (K)	95	95
Detector	EIGER X4M	PILATUS3 S6M
Space group	$P2_12_12$	
Unit-cell parameters (Å, °)	a = 90.4, b = 154.2, c = 82.7, $\alpha = \beta = \gamma$ = 90	
Resolution range (Å)	48.2–2.74 (2.81–2.74)	50.0–2.1 (2.14 2.10)
No. of unique reflections	56880 (2432)	69549 (3426)
Multiplicity	5.8 (1.4)	6.7 (6.9)
Completeness (%)	95.0 (55.2)	98.9 (98.0)
$\langle I/\sigma(I)\rangle$	16.56 (3.3)	24.9 (2.5)
R_{merge}	0.086 (0.214)	0.070 (0.529)
Refinement		
Resolution range (Å)		43.6–2.1 (2.14–2.10)
Completeness (%)		98.4 (92.1)
No. of reflections		66018 (4732)
R_{work}		0.217 (0.271)
R_{free}		0.231 (0.301)
No. of non-H atoms		
Protein		7342
Water		125
Phosphate		5
R.m.s. deviations		
Bonds (Å)		0.010
Angles (°)		1.462
Average B factors (Å^2)		
Protein		38.6
Water		39.3
Phosphate		48.5
Ramachandran plot		
Favoured (%)		98.4
Allowed (%)		1.6
Disallowed (%)		0

2.2. Crystallization

Crystallization was performed by the hanging-drop vapour-diffusion method at 20°C using drops consisting of 1 µl protein solution and reservoir solution. Rhombic-shaped crystals were obtained with a reservoir solution containing only 1 *M* $(NH_4)_2HPO_4$ after one week. However, they were very thin plates and produced poor diffraction patterns. Therefore, we tried the counter-diffusion method using the Granada Crystallization Box (Hampton Research). After three weeks, thick rhombic-shaped crystals were obtained in a capillary, which were suitable for data collection. For data collection, the

reservoir buffer was replaced with the same buffer containing 25% glycerol and left to diffuse for one week.

2.3. Data collection, processing and model building

Diffraction data were obtained on BL-1A (Liebschner *et al.*, 2016) equipped with an EIGER X4M pixel-array detector and on BL-17A (Igarashi *et al.*, 2007) equipped with a PILATUS3 S6M (Dectris) at the Photon Factory, High Energy Accelerator Research Organization, Tsukuba, Japan. Data sets were collected at 95 K in helium-gas and nitrogen-gas cryostreams on BL-1A and BL-17A, respectively. A 2.1 Å resolution data set was collected on BL-17A and was processed using *HKL*-2000 (Otwinowski & Minor, 1997). Molecular replacement was carried out using *MoRDa* (A. Vagin & A. Lebedev; http://www.biomexsolutions.co.uk/morda), but only a partial model was obtained which corresponded to the substrate-binding domains. For a native SAD data collection, diffraction data consisting of 3600 images were collected from a single crystal with a wavelength of 2.7 Å on BL-1A, with an oscillation

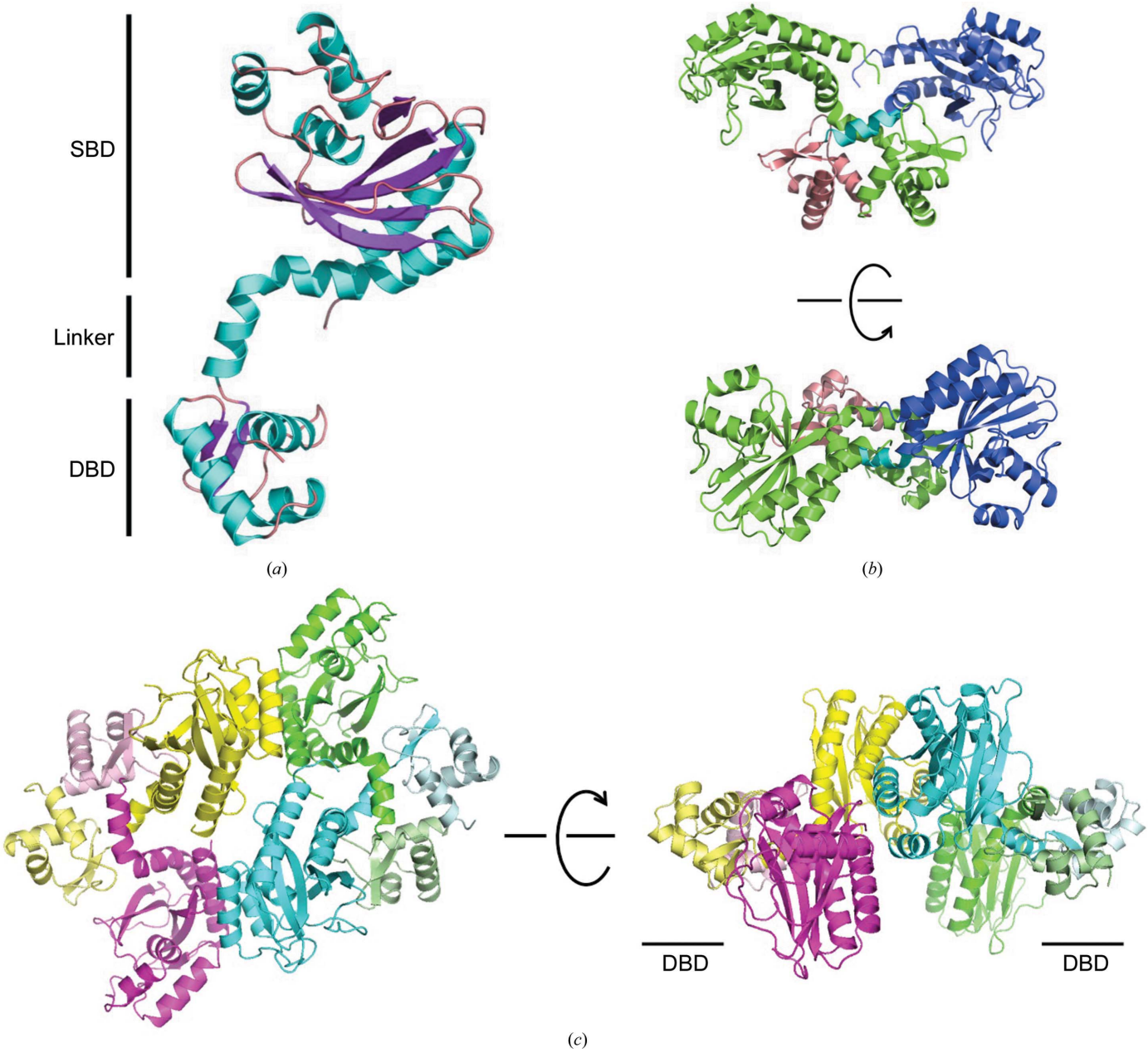

Figure 1
Overall structure of Mi-IclR. (*a*) A subunit consists of a DNA-binding domain (DBD) at the N-terminus and a substrate-binding domain (SBD) at the C-terminus. Secondary structures are coloured cyan and magenta for α-helices and β-sheets, respectively. (*b*) Front view (top) and top view from the SBD side (bottom) of the homodimer conformation of Mi-IclR. One of the subunits in the dimer is coloured blue, cyan and pink for the SBD, the linker and the DBD, respectively. (*c*) Top view (left) and side view (right) of the homotetramer structure of Mi-IclR. The four subunits are shown in different colours, and the DBDs are indicated in the cognate pale colours.

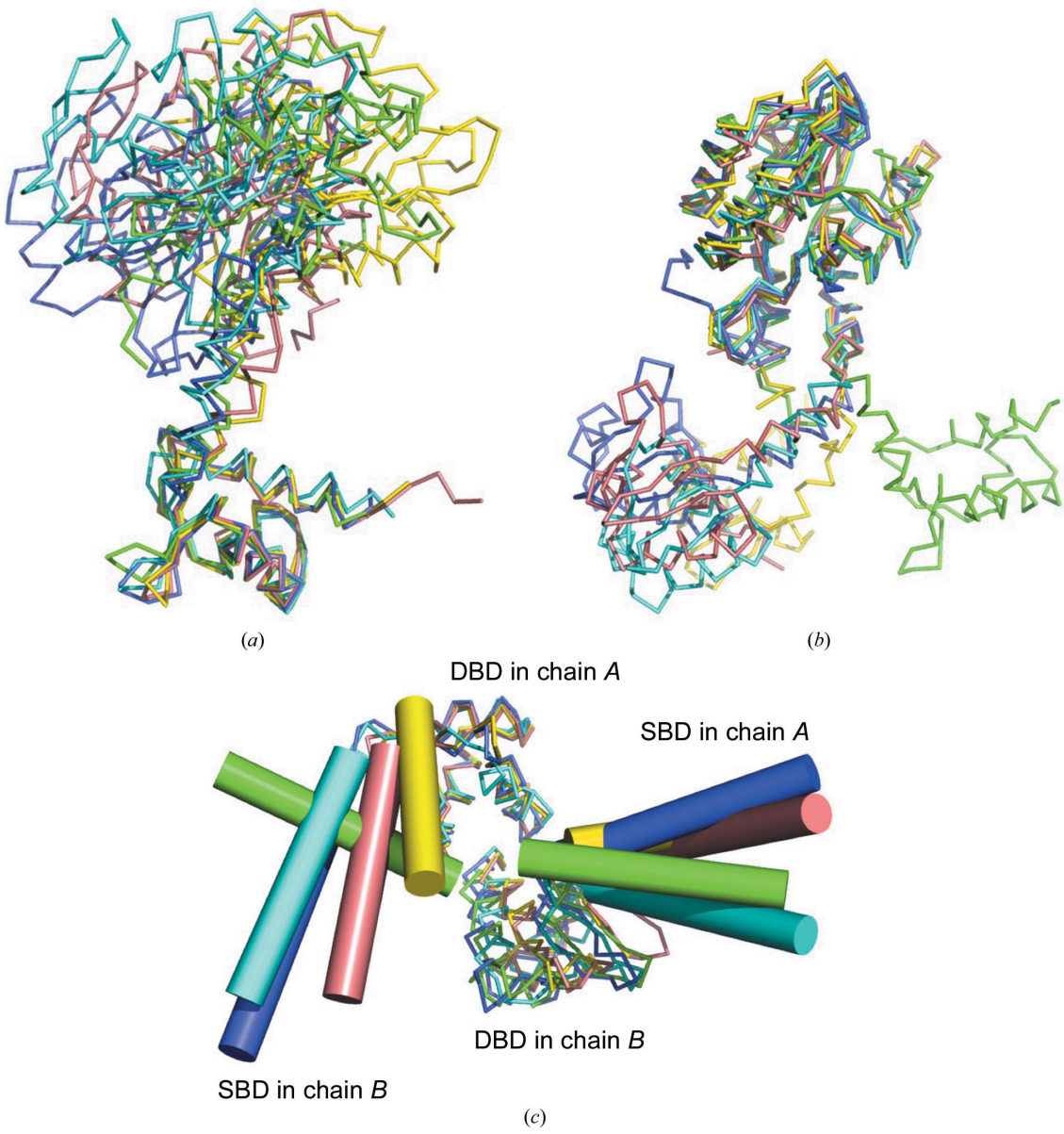

Figure 2
Superposition of Mi-IclR with four known IclR structures. Superposition of four IclRs (coloured cyan, pink, yellow and blue for PDB entries 1mkm, 2g7u, 2ia2 and 3r4k, respectively) with Mi-IclR (coloured green) was performed and C^{α} traces are presented. Superpositions on the DBD (*a*) and the SBD (*b*) were performed using *LSQKAB* and *Chimera*, respectively. (*c*) The dimer structures were compared by superposition of the DBDs in chains *A*. The DBDs are shown as a C^{α}-trace model and the SBDs as a cartoon model. Only the C-terminal helix of each SBD is presented. The same colours are used as in (*a*) and (*b*).

width of 0.1° and 0.1 s exposure per image. The collected data were merged and scaled using the *XDS* package (Kabsch, 2010). To obtain a complete structure, the MR-SAD technique was applied using *CRANK*2 (Skubák & Pannu, 2013) running with *SFTOOLS*, *REFMAC*5, *PEAKMAX*, *Parrot* and *Buccaneer* in the *CCP*4 suite (Winn *et al.*, 2011). Iterative refinement and model building were performed by *REFMAC*5 (Murshudov *et al.*, 2011) and *Coot* (Emsley *et al.*, 2010), respectively. Figures were prepared using *PyMOL* (Schrödinger). The atomic coordinates and structure factors have been deposited in the RCSB Protein Data Bank with accession code 5h1a.

3. Results and discussion

3.1. Structure determination

The crystal of Mi-IclR belonged to space group $P2_12_12$, with unit-cell parameters $a = 90.4$, $b = 154.2$, $c = 82.7$ Å. Initially, we obtained a thin plate-shaped crystal using the hanging-drop vapour-diffusion method. This crystal only produced weak diffraction patterns with high anisotropy. We then tried the counter-diffusion method and succeeded in obtaining thicker crystals, which produced diffraction to 2.1 Å resolution, although it was difficult to obtain this resolution for all crystals. The amino-acid sequence identity between Mi-IclR and

structurally determined IclRs is 21, 22, 22 and 25% for PDB entries 1mkm, 2g7u, 3r4k and 2ia2, respectively (Supplementary Fig. S1). The overall structures of the IclRs are almost identical to each other and are composed of a DNA-binding domain (DBD) at the N-terminus and a substrate-binding domain (SBD) at the C-terminus, with a connecting short α-helix. Based on the amino-acid sequence identities given above, our first attempt to obtain an initial model used the molecular-replacement method. Although *MOLREP* (Vagin & Teplyakov, 2010) and *Phaser* (McCoy *et al.*, 2007) failed to provide solutions, *MoRDa* gave a solution as a collection of domains: four SBDs and two DBDs. However, of these only two SBDs fitted to the electron-density map. Using these partial structures, we then applied the MR/native SAD technique using a data set collected with a wavelength of 2.7 Å.

The IclR expression construct in this study contains seven Met residues from the IclR sequence and one from the vector sequence, but there are no Cys residues in the 250 residues in a subunit; the asymmetric unit contains four IclR subunits. The two SBDs (Arg83–Arg249) obtained by *MoRDa* contained two Met residues in each and were used as a partial model for input to *CRANK*2; *PEAKMAX* found seven peaks in the anomalous difference density map. Owing to the geometry of the diffractometer, complete data could not be collected at a resolution higher than 2.9 Å. However, these incomplete high-resolution data were necessary to solve the structure. Finally, *CRANK*2 automatically built the model of four subunits of IclR in an asymmetric unit with an R and $R_{\rm free}$ of 0.239 and 0.304, respectively, and 972 residues. The modelled structure was further refined by *REFMAC*5. Data-collection and refinement statistics are summarized in Table 1.

3.2. Overall and subunit structure

Similar to other IclRs reported in the PDB, a subunit of Mi-IclR comprises an HTH-type DBD (residues Met1–Leu67; coloured pink in Fig. 1*b*) at the N-terminus connected by a short α-helix (Gly68–Gly78; coloured cyan) to the SBD (Ser79–Trp250; coloured blue) at the C-terminus. There are four subunits of Mi-IclR in the asymmetric unit, which comprise a dimer of dimers. An X-shaped homodimer is formed by two subunits crossing at the linker helix (Fig. 1*b*). Two homodimers face each other on the SBD, which results in exposure of the DBDs to the outside of the homotetramer structure (Fig. 1*c*).

Since all full-length IclR structures in the PDB as well as Mi-IclR adopt an identical combination of domains, we compared the Mi-IclR structure with those of four other IclRs. Superpositions of the DBDs of Mi-IclR and the four other IclRs show a good fit, with root-mean-square deviations (r.m.s.d.s) of 1.86, 1.15, 0.92 and 0.94 Å calculated by *LSQKAB* (Kabsch, 1976) in the *CCP*4 suite for PDB entries 1mkm (residues Lys5–Arg52), 2g7u (Glu13–Gly60), 2ia2 (Ala21–Thr68) and 3r4k (Ser5–Gln52), respectively, against Mi-IclR (residues Ala12–Arg59) (Fig. 2*a*). A superposition of the SBDs also showed a good fit, with r.m.s.d.s of 1.07, 1.12, 1.00 and 1.04 Å calculated by *Chimera* (Pettersen *et al.*, 2004) for PDB entries 1mkm, 2g7u, 2ia2 and 3r4k, respectively (Fig. 2*b*). Since the number of residues in the C-terminal domains differed among the five IclRs, *Chimera* was used instead of *LSQKAB*. *Chimera* creates a pairwise sequence alignment and then calculates r.m.s.d.s for aligned residues. Interestingly, superposition of the SBDs revealed remarkable differences between the five structures, in which the DBD of Mi-IclR was directed in a different orientation compared with those of the other IclRs (Fig. 2*b*). We then compared the dimer structures. When the DBDs in chains *A* were superposed, only the SBD of Mi-IclR showed a different geometry from those of the other four IclRs (Fig. 2*c*). Although only *T. maritima* IclR (TM-IclR) is known to form a tetramer in solution (Zhang *et al.*, 2002), and the oligomerization states of

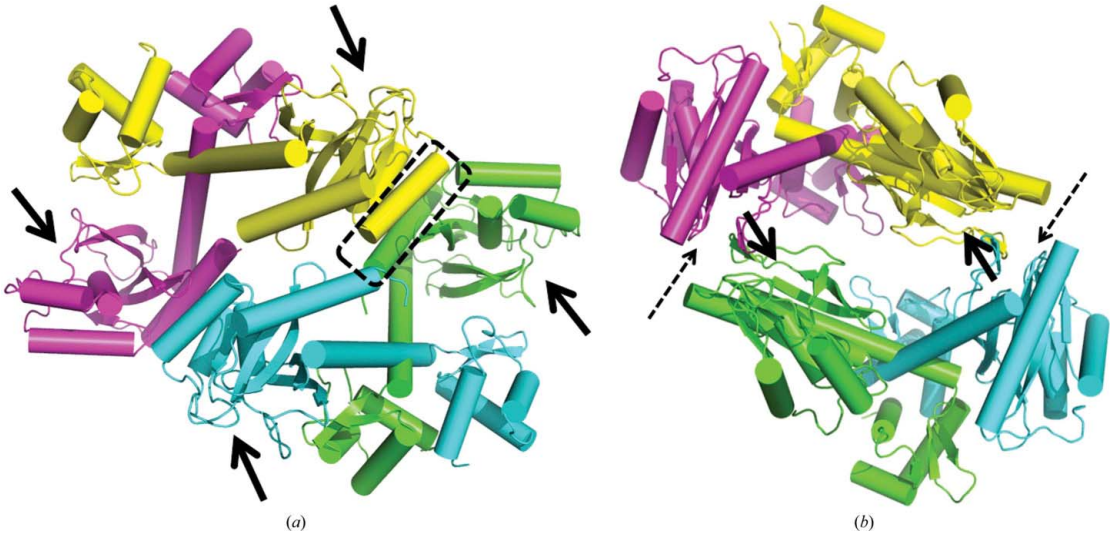

Figure 3
Comparison of the geometry of the homotetramer. The geometry of the homotetramer was compared between Mi-IclR (*a*) and IclR from *Silicibacter* sp. (PDB entry 3r4k) (*b*). Arrows indicate the entrances to the putative substrate-binding sites, and broken-lined arrows show that the entrances open to the back side. The region surrounded by the dotted line is enlarged and presented in Fig. 4.

the rest of the IclRs, including Mi-IclR, are not known, if these IclRs form tetrameric structures then the differences in the geometry of the dimers could affect the tetramer structures accordingly as described below.

3.3. The tetramer structure of Mi-IclR

According to the subunit structure, the geometry of the tetramer of Mi-IclR shows distinct differences from those of the other IclRs. As shown in Fig. 3(*a*), in Mi-IclR the putative substrate-binding sites are accessible from the outside of the tetramer. On the other hand, in the IclR structure with a tetramer in the asymmetric unit from *Silicibacter* sp. TM1040 (PDB entry 3r4k), the space group of which is identical to that of Mi-IclR, the putative substrate-binding site of one subunit in each dimer is buried inside of the tetramer at the dimer–dimer interface (Fig. 3*b*). All other IclR structures in the PDB, PDB entries 1mkm (space group *C*2), 2ia2 ($P2_12_12_1$) and 2g7u ($C222_1$), also adopt the same geometry of the tetramer as that of PDB entry 3r4k, in which half of the putative substrate-binding sites face the dimer–dimer interface.

The dimer–dimer interaction in Mi-IclR is established mainly by Arg and Glu residues, which comprise 17 and 16 out of 172 residues in the SBD, respectively. As shown in Fig. 4, Arg residues form hydrogen bonds and salt bridges: Arg208 in chain *A*–Glu175 in chain *D*, Glu210 in chain *A*–Arg186 in chain *D*, Glu242 in chain *A*–Arg155 in chain *D*, Arg246 in chain *A*–Ala150 (carbonyl) in chain *D* and Arg249 in chain *A*–Tyr185 in chain *D*. Arg208 in chain *A* also makes hydrophobic interactions with Glu156 and Arg178 in chain *D*. Arg246 in chain *B* dimerizes with chain *A* and also interacts with the backbone O atom of Tyr185 in chain *D*. When we performed a sequence alignment based on the superposition of IclRs with Mi-IclR using *Chimera*, no consensus residues were observed amongst those involved in the dimer–dimer interaction in Mi-IclR except for Glu156 and Arg178. Therefore, other IclRs may be unable to adopt the geometry of the tetramer observed for Mi-IclR. On the other hand, other IclRs use hydrophobic interactions to form a tetramer, and the corresponding residues are conserved as Ala124, Val125, Leu128, Ala129, Val131, Ile196 and Val199 in Mi-IclR.

Since Mi-IclR works under aqueous conditions in cells, the ionic interactions may not be strong enough to form a stable tetramer. The possibility of a crystal-packing effect on the geometry of this tetramer therefore cannot be excluded. TM-IclR is considered to be a dimer in the absence of a ligand and DNA, but adopts a tetrameric structure when bound to DNA in the absence of a ligand (Zhang *et al.*, 2002). *E. coli* IclR forms a stable tetramer with a small amount of dimer, and a more stable tetramer with DNA (Donald *et al.*, 2001). Therefore, Mi-IclR is also expected to form a tetramer in cells.

The nucleotide sequences bound by IclRs share no consensus but consist of palindromic, inverted or direct repeats (Molina-Henares *et al.*, 2006). Zhang and coworkers modelled the DNA complex with TM-IclR, in which the two dimeric DBDs aligned approximately linearly, based on the geometry of the tetramer (Fig. 5*a*; Zhang *et al.*, 2002). On the other hand, the two dimeric DBDs in Mi-IclR are distant from each other because the tetramer is composed of a head-to-head arrangement of two dimers (Fig. 5*b*). Therefore, if this structure exists in cells, Mi-IclR may bind to two DNA sites

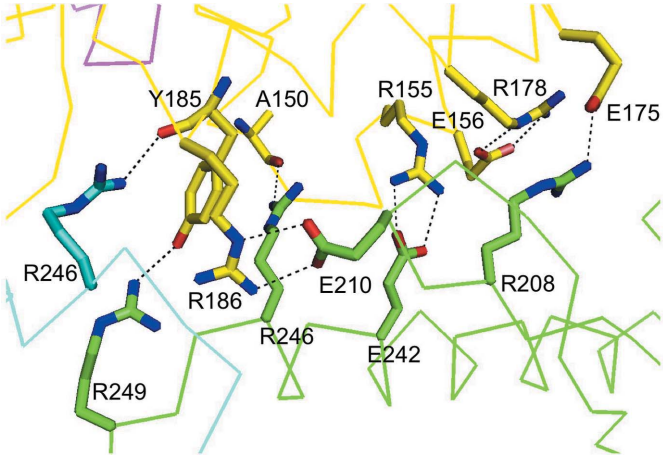

Figure 4
The dimer–dimer interface of Mi-IclR. The interactions in the dimer interface between chain *A* (coloured green) in one dimer and chain *D* (coloured yellow) in the other dimer are presented. Dotted lines show distances that are less than 3.0 Å, with the exception of 3.2 Å between Arg246 in chain *B* (coloured cyan) and Tyr185 in chain *D*.

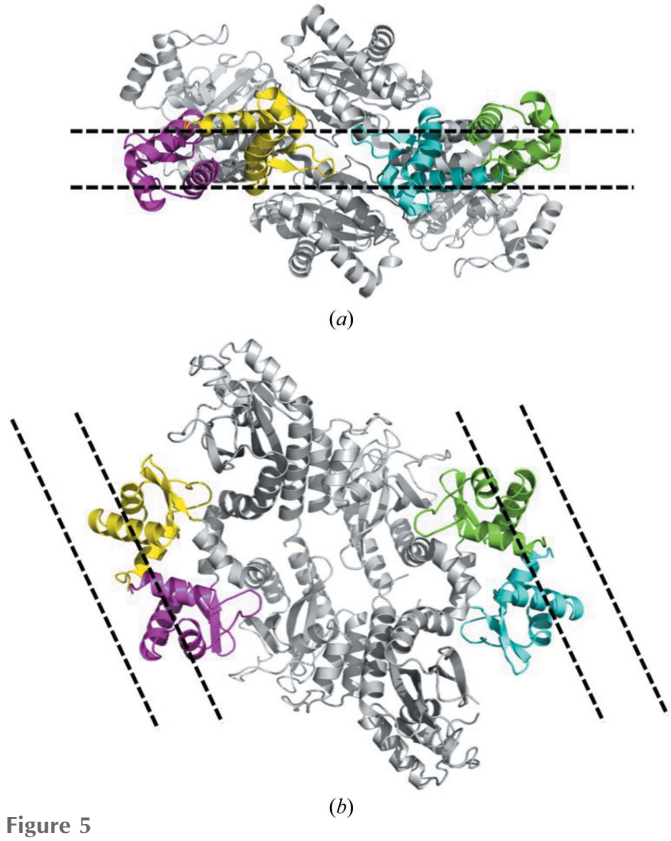

Figure 5
A model of DNA binding. A tetrameric structure was postulated on DNA binding. (*a*) Based on the report by Zhang and coworkers on IclR from *T. maritima*, the dimeric DNA-binding domains align side by side and bind to DNA. (*b*) The two dimeric DNA-binding domains of Mi-IclR are distant from each other; therefore, the binding targets are also located with a long separation on the DNA. The parallel dotted lines indicate double-helix DNA.

which are located far apart, although no binding sequences have yet been identified.

IclR acts as either a repressor or an activator, and is expected to change the DNA-binding mode by its conformational change in response to the binding of a specific substrate. Therefore, the conformational differences of the tetramers between Mi-IclR and other IclRs may reflect two modes corresponding to 'on' and 'off' functions of IclRs, although Mi-IclR may be categorized into a different group to the other IclR structures.

Additionally, when the SBD in chain *A* in the dimer of Mi-IclR was superposed with that of TM-IclR, the other SBDs in chain *B* was positioned quite differently (Fig. 6). This could also suggest a conformational change on the regulation of the transcriptional activities by IclRs.

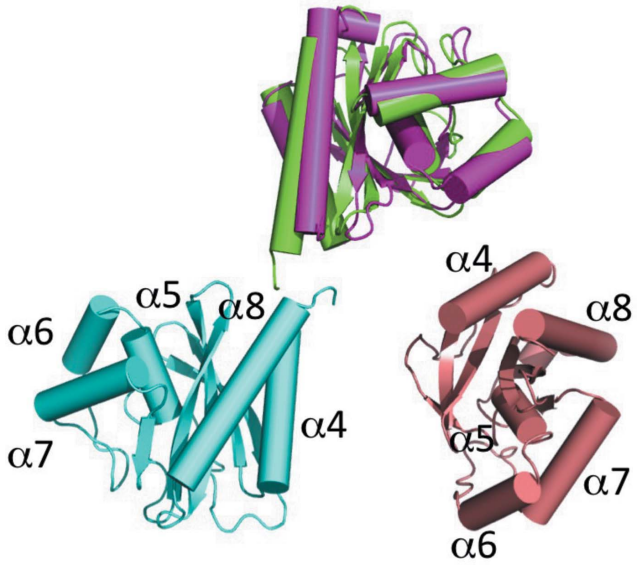

Figure 6
Superposition of SBDs in the dimer structure. The SBD in chain *A* in the dimer of Mi-IclR was superposed on that of TM-IclR. The SBDs of Mi-IclR are coloured green and cyan for chains *A* and *B*, respectively. Those of TM-IclR are coloured magenta and pink for chains *A* and *B*, respectively.

3.4. Structure of the substrate-binding domain

When we superposed the SBD of Mi-IclR with that of *E. coli* IclR complexed with pyruvate, both fitted well overall, with an r.m.s.d. of 1.15 Å calculated by *Chimera*. However, a marked difference was observed in the loop region (His122–His138), which covers a putative substrate-binding site in Mi-IclR. On the other hand, in *E. coli* IclR this region (Thr141–Met156) adopts an open position over the substrate (Fig. 7*a*). In the Mi-IclR structure in particular, the electron density in this region was unclear, and as a result part of this region in chain *A* was not modelled. This result therefore suggests that this loop region has flexibility for substrate binding.

The acylhydrazide compound HBPH used as the sole carbon source for the growth of strain HM58-2 is a rather large molecule compared with pyruvate or glyoxylate. When we

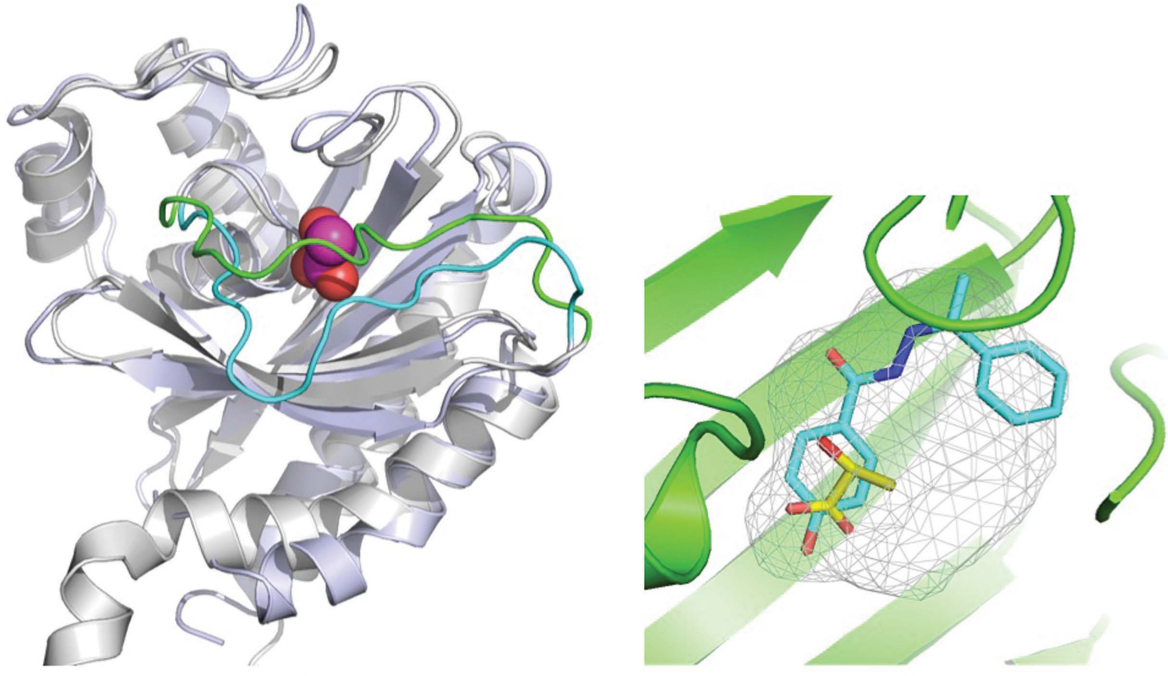

(*a*) (*b*)

Figure 7
Comparison of the substrate-binding domain. (*a*) The substrate-binding domain of IclR was superposed with that of *E. coli* IclR complexed with pyruvate. Both structures fitted well except for the loop regions coloured green and cyan for Mi-IclR and *E. coli* IclR, respectively. Pyruvate in *E. coli* IclR is presented as a sphere model. (*b*) The putative substrate-binding pocket of Mi-IclR. The pocket cavity was calculated by *PyMOL* and is presented as a grey mesh. HBPH is represented by a stick model coloured cyan. The pyruvate molecule coloured yellow is located where the SBD of *E. coli* IclR (PDB entry 2o9a) and that of Mi-IclR are superposed.

placed HBPH in the putative binding site manually, the molecule almost fits into the site (Fig. 7*b*). In this position, it could be possible to make a hydrophobic interaction between the phenyl group of HBPH and Ile196, whereas a backbone carbonyl O atom is located in proximity. HBPH is degraded to 4-hydroxybenzoic acid (HBA) and acetophenone hydrazone by the hydrazidase produced by strain MH58-2, and HBA is considered to be the carbon source for bacterial growth. Therefore, further study is necessary in order to determine the ligand(s) of Mi-IclR.

4. Conclusion

In this study, we solved the crystal structure of an IclR homologue from *Microbacterium* sp. HM58-2 using the MR/native SAD method. The structures of the domain components of the subunit were similar to those of known IclR structures. On the other hand, the oligomer conformation was significantly different. These differences may lead to the elucidation of the function of IclR in the regulation of bacterial metabolism.

Acknowledgements

We are grateful to the beamline staff at the Photon Factory for their technical support. We also thank Dr Miki Senda at the Structural Biology Research Center, KEK for discussion of the MR/native SAD technique. This project was supported by JSPS KAKENHI Grant No. 15K07369 (to SY) and partially supported by the Platform Project for Supporting in Drug Discovery and Life Science Research (Platform for Drug Discovery, Informatics and Structural Life Science) from the Japan Agency for Medical Research and Development (AMED) (to YY).

References

Akiyama, T., Ishige, T., Kanesaki, Y., Ito, S., Oinuma, K., Takaya, N., Sasaki, Y. & Yajima, S. (2016). *Genome Announc.* **4**, e00554-16.
Donald, L. J., Hosfield, D. J., Cuvelier, S. L., Ens, W., Standing, K. G. & Duckworth, H. W. (2001). *Protein Sci.* **10**, 1370–1380.
Emsley, P., Lohkamp, B., Scott, W. G. & Cowtan, K. (2010). *Acta Cryst.* D**66**, 486–501.
Gui, L., Sunnarborg, A., Pan, B. & LaPorte, D. C. (1996). *J. Bacteriol.* **178**, 321–324.
Igarashi, N., Matsugaki, N., Yamada, Y., Hiraki, M., Koyama, A., Hirano, K., Miyoshi, T. & Wakatsuki, S. (2007). *AIP Conf. Proc.* **879**, 812–815.
Kabsch, W. (1976). *Acta Cryst.* A**32**, 922–923.
Kabsch, W. (2010). *Acta Cryst.* D**66**, 125–132.
Krell, T., Molina-Henares, A. J. & Ramos, J. L. (2006). *Protein Sci.* **15**, 1207–1213.
Levenberg, B. (1964). *J. Biol. Chem.* **239**, 2267–2273.
Liebschner, D., Yamada, Y., Matsugaki, N., Senda, M. & Senda, T. (2016). *Acta Cryst.* D**72**, 728–741.
López-Muñoz, F., Álamo, C., Juckel, G. & Assion, H. J. (2007). *J. Clin. Psychopharmacol.* **27**, 555–559.
Lorca, G. L., Ezersky, A., Lunin, V. V., Walker, J. R., Altamentova, S., Evdokimova, E., Vedadi, M., Bochkarev, A. & Savchenko, A. (2007). *J. Biol. Chem.* **282**, 16476–16491.
McCoy, A. J., Grosse-Kunstleve, R. W., Adams, P. D., Winn, M. D., Storoni, L. C. & Read, R. J. (2007). *J. Appl. Cryst.* **40**, 658–674.
Michelot, D. & Toth, B. (1991). *J. Appl. Toxicol.* **11**, 235–243.
Molina-Henares, A. J., Krell, T., Guazzaroni, M. E., Segura, A. & Ramos, J. L. (2006). *FEMS Microbiol. Rev.* **30**, 157–186.
Murshudov, G. N., Skubák, P., Lebedev, A. A., Pannu, N. S., Steiner, R. A., Nicholls, R. A., Winn, M. D., Long, F. & Vagin, A. A. (2011). *Acta Cryst.* D**67**, 355–367.
Oinuma, K., Takuwa, A., Taniyama, K., Doi, Y. & Takaya, N. (2015). *J. Bacteriol.* **197**, 1115–1124.
Otwinowski, Z. & Minor, W. (1997). *Methods Enzymol.* **276**, 307–326.
Pettersen, E. F., Goddard, T. D., Huang, C. C., Couch, G. S., Greenblatt, D. M., Meng, E. C. & Ferrin, T. E. (2004). *J. Comput. Chem.* **25**, 1605–1612.
Scior, T., Meneses Morales, I., Garcés Eisele, S. J., Domeyer, D. & Laufer, S. (2002). *Arch. Pharm. Pharm. Med. Chem.* **335**, 511–525.
Skubák, P. & Pannu, N. S. (2013). *Nature Commun.* **4**, 2777.
Stock, A. M., Robinson, V. L. & Goudreau, P. N. (2000). *Annu. Rev. Biochem.* **69**, 183–215.
Sunnarborg, A., Klumpp, D., Chung, T. & LaPorte, D. C. (1990). *J. Bacteriol.* **172**, 2642–2649.
Ulrich, L. E., Koonin, E. V. & Zhulin, I. B. (2005). *Trends Microbiol.* **13**, 52–56.
Vagin, A. & Teplyakov, A. (2010). *Acta Cryst.* D**66**, 22–25.
Winn, M. D. *et al.* (2011). *Acta Cryst.* D**67**, 235–242.
Zhang, R., Kim, Y., Skarina, T., Beasley, S., Laskowski, R., Arrowsmith, C., Edwards, A., Joachimiak, A. & Savchenko, A. (2002). *J. Biol. Chem.* **277**, 19183–19190.